

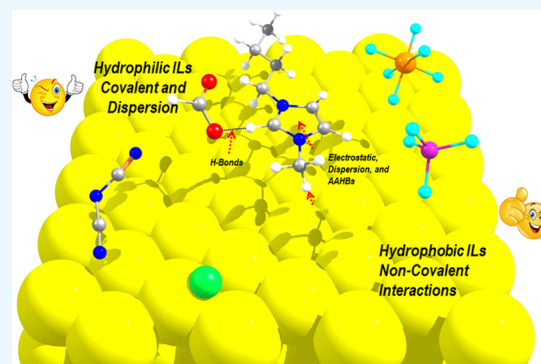
Adsorption of Hydrophobic and Hydrophilic Ionic Liquids at the Au(111) Surface

Shanmugasundaram Kamalakannan,[†] Muthuramalingam Prakash,^{*,†,‡,§} Gilberte Chambaud,[§] and Majdi Hochlaf^{*,§}

[†]Department of Chemistry and [‡]SRM Research Institute, SRM Institute of Science and Technology, Kattankulathur 603203, Tamil Nadu, India

[§]Laboratoire Modélisation et Simulation Multi Echelle, MSME UMR 8208 CNRS, Université Paris-Est, 77454 Marne la Vallée Cedex 2, France

ABSTRACT: Electrode–electrolyte microscopic interfacial studies are of great interest for the design and development of functional materials for energy storage and catalysis applications. First-principles-based simulation methods are used here to understand the structure, stability, energetics, and microscopic adsorption mechanism of various hydrophilic and hydrophobic ionic liquids (ILs; 1-butyl 3-methylimidazolium [BMIm]⁺[X]⁻, where X = Cl, DCA, HCOO, BF₄, PF₆, CH₃SO₃, OTF, and TFSA) interacting with a metallic surface. We have selected the Au(111) surface as a potential electrode model, and our computations show that ILs (anions and cations) adsorb specifically at some selective adsorption sites. Indeed, hydrophilic anions of ILs are strongly adsorbed on the gold surface (via Au–Cl and Au–N bonds at Au(111)), whereas hydrophobic anions are weakly bonded. The [BMIm]⁺ is always found to be stabilized parallel to the metal surface, irrespective of the nature of the anion, through various kinds of noncovalent interactions. Mulliken, Löwdin, and Hirshfeld charge analyses reveal that there is significant charge transfer between ILs and the surface that may enhance the charge transfer mechanism between the surface and electrolytes for electrochemical applications. Our study shows that the electrostatic and van der Waals interactions are in action at these interfaces. Moreover, we show that there are several covalent and noncovalent interactions between ILs and the metal surface. These interactions play an essential role to maintain the electrostatic behaviors at the solid–liquid interface. The present findings can be helpful to predict specific selectivity and subsequent design of materials for energy harvesting and catalysis applications.



1. INTRODUCTION

The electrode–electrolyte interface studies are of great importance to understand the interfacial phenomena for the design and development of functional materials for various applications such as supercapacitors, batteries, and catalysis.^{1,2} Several experimental and theoretical works have been devoted to the understanding of the interfacial structure and reactivity of molecules at these interfaces.^{3–5} Particularly, allotropes of carbon (i.e., graphene, carbon nanotube, fullerene, etc.) interacting with ionic liquid (IL) electrolytes received special attention because these materials present potential applications for energy storage in Li-ion batteries, supercapacitors, and lubricants and as anticorrosive.^{6–12} More generally, these investigations aim to tackle new challenges to elucidate the energy storage mechanisms and to enhance the storage capacities.^{13,14}

Room-temperature ionic liquids (RTILs) are mainly composed of organic cations and inorganic anions. The great interest in these ILs stems from their specific properties such as high ionic conductivity,¹⁵ nonflammability,¹⁶ high thermal stability,¹⁷ low vapor pressure, and wide electrochemical window.¹⁸ Moreover, the behavior of RTILs at charged

surfaces can be used toward the applications of supercapacitors,¹⁹ of electrochemical sensors,²⁰ in catalysis,²¹ and in energy storage.²² This is mainly due to the electrostatic interaction between electrode and electrolyte surfaces and to the formation of a second layer of ILs in the vicinity of these surfaces. These structures are known as electrical double layer (EDL).²³ The EDL part of composites plays an essential role in the energy storage and conversion.

Two-dimensional (2D) metal-surface-based electrode materials are also potential candidates for applications of energy storage devices.²⁴ Al, Ni, Pt, and noble metals such as Cu, Ag, and Au are of prime importance as materials for such devices.^{25–31} Among these composite materials, Au atoms on the electrode surface are good candidates because they have higher surface atom density and stronger van der Waals (vdWs) interactions than those of the other metallic surfaces.³²

Gold surface Au(111)–IL composite materials (i.e., ILs@Au(111)) exhibit high conductivity, high thermal and chemical

Received: August 24, 2018

Accepted: December 6, 2018

Published: December 21, 2018

stabilities, and compatibility for material design.³³ Thus, they are commonly used as an electrode–electrolyte model. Moreover, it is established that these composites improve the performance of printed circuit boards when compared to that of other electrode materials (e.g., Ag).³⁴

Recent theoretical studies predicted the importance of regium bond between coinage metal clusters and aromatic π -systems and N-based nucleophiles.^{35,36} These studies revealed that the strength of the interaction between these complexes mainly follow the basicity of the nucleophiles and the calculated regium bond energies are above ~ 30 kcal/mol. However, aromatic system energies range from ~ 7 to 30 kcal/mol. Particularly, gold complexes achieved strong binding than the other metals. This shows that gold metal plays an important role in molecular adsorption and catalytic applications, which is important to understand the adsorption mechanism at the microscopic level. This is in line with our findings on ILs at Au(111) surfaces because of the strong adsorption of both the alkyl chain and the cationic part of the imidazolium ring.

To understand the effect of anions–cations in ILs and the adsorption mechanism of the alkyl chain, several studies dealing with gold–IL interfaces have been reported.^{37–44} For instance, Pan et al. observed a 2D phase transition of PF₆ adlayers at the electrified Au(111)–IL interface using the *in situ* scanning tunneling microscope (STM) technique. After application of positive potential, they showed the formation of surface etching and ordered adlayers at the Au(111) electrode. This is attributed to different solvation effects of PF₆ in ionic liquids compared to those in aqueous solution.³⁸ Moreover, Maier and co-workers studied the adsorption behavior, orientation, and growth of ILs on the Au(111) surface using angle-resolved X-ray photoelectron spectroscopy (XPS). Their work pointed out the arrangement of 1,1-dimethylimidazolium-bis(trifluoromethylsulfonyl)imide ([MMIm]⁺[TFSA]⁻) and 1-octyl-3-methylimidazolium ([OMIm]⁺[TFSA]⁻) on the Au(111) surface.³⁹ Later on, Wen et al. studied the molecular arrangement and surface dynamics of different ILs ((hexyl-3-methylimidazolium bis(trifluoromethylsulfonyl)-imide HMIm)⁺ with Cl⁻ and [TFSA]⁻) at the Au(111) surface using *in situ* high-speed STM. They found a possible dependent adlayer structure of adsorbed [HMIm]⁺ and [Cl]⁻ at the gold surface.⁴⁰ The elucidation of such effect is among the aims of the present first-principles investigations.

Recently, the influence of alkyl chains in the cations at the Au(100) and Au(111) surfaces was studied by experimental techniques.^{41,42} The *in situ* STM study revealed the formation of an ordered “micellelike” structure at the Au(100) surface and of irregular “wormlike” structure at the Au(111) surface. Su et al. performed an STM study of BMIm-BF₄@Au(111) (solid–liquid interface) over a wide range of potentials. This potential-dependent study gives independent assessment of the position of the point of zero charge.⁴³ More recently, Uhl et al. elucidated the adsorption of [EMIm]⁺[TFSA]⁻ and [OMIm]⁺[TFSA]⁻ at Au(111). Again, they identified the formation of an adlayer on the surface and the influence of cation and anion upon adsorption.⁴⁴ Tamura and Nishihata used X-ray scattering to study the behavior of halide ions on the ILs@Au(111) electrode, where IL = 1-butyl-1-methylpyrrolidinium ([BMP]⁺[TFSA]⁻) and ([BMIm]⁺[TFSA]⁻). They concluded that the adsorption of [BMP]⁺[TFSA]⁻ and [BMIm]⁺[TFSA]⁻ is stronger than that of the halide ions. They revealed also that the interfacial structure is influenced

not only by the concentration of ILs but also by the nature of the anions and cations in the composition of the ILs.⁴⁵ In brief, these investigations established that the adsorption of anions and cations at the gold surface can significantly affect the chemical reactivity of the electrode.⁴⁶

At the molecular level, more light can be shed onto the adsorption mechanism, reactivity, and the ordering of various ILs at metal surfaces using quantum chemical calculations and molecular dynamics with the help of force-field-based simulations. Indeed, recent advances in molecular modeling showed that these techniques represent a valuable tool to predict the nanoscale properties and reactivity at these material interfaces and the adsorption mechanism and physical properties of ILs at 2D surfaces.⁴⁷ For instance, Mendonca et al. reported the ordering of ILs@Fe surface using density-functional-based force-field calculations to study the effect of the adsorption of short- and long-chain alkyl groups in ILs. Moreover, their molecular dynamics (MD) simulations revealed that both the anion and the cation of the ILs are adsorbed on the Fe surface and that the oxygen atom of the sulfonyl group is particularly strongly bonded with the metal. They also found that the interfacial layer is composed of a unique layer except for the very short chain alkyl groups where a second layer is formed. Different behaviors are noticed for butyl chains of the sulfonate anions (which tend to be directed away from the surface) and ammonium cations (lying more parallel to the surface).⁴⁸ Later on, Heinz and co-workers reported facet recognition and molecular ordering of 1-ethyl-3-methylimidazolium ethyl sulfate ([EMIm]⁺[ES]⁻) on the Au(111), Au(100), and Au(110) surfaces employing quantum mechanical and classical simulation approaches. They identified self-assembly of ILs@gold surfaces from single ion pairs to multilayers. They showed that adsorption is controlled by the interplay of soft epitaxy, ionic interactions, induced charges, and steric effects related to the geometry of the cation and the anion.⁴⁹ These findings are also observed for ILs in Au nanopores. Indeed, orientation and confined effects of 1-butyl-3-methylimidazolium hexafluorophosphate ([BMIm]⁺[PF₆]⁻) IL at Au nanopores were pointed out after MD simulations by Liu et al.⁵⁰ Their study stated also that the Im ring of [BMIm]⁺ prefers to form a small tilt angle with the pore walls and that the dynamics of confined ILs is remarkably slower than that observed in the bulk phase. Nevertheless, there is evident lack of understanding, at the microscopic level, the charge transfer mechanisms and the adsorption sites on surfaces. This may be connected to the fact that pure first-principles investigations of ILs on metals and more specifically on gold surfaces are rare in contrast to the large number of experimental studies. We can cite for instance the work of Ploger et al. who used the periodic density functional theory (DFT) approach to elucidate the coverage of the surface of Au(100) by [BMIm]⁺[PF₆]⁻ and their respective orientation with a wide range of coverage.⁵¹

Beattie et al.⁵² reported the adsorption behavior of 0.1% 1-[HMIm]⁺[NTf₂]⁻; (NTf₂ also called TFSI), in ethanol solutions, onto the gold surface using XPS and spectroscopic ellipsometry methods. They found that both anions and cations are present in the surface-bound layer and also that the adsorbed layer thickness (of ~ 1.5 Å) is smaller than the size of an IL ion pair. Very recently, the same group studied [HMIm]⁺ with [NTf₂]⁻ and [Cl]⁻ anions on silver (Ag) using synchrotron-based XPS spectroscopy. They showed that there is no chemical interaction between the [HMIm]⁺[NTf₂]⁻ pair and Ag, whereas a chemical interaction

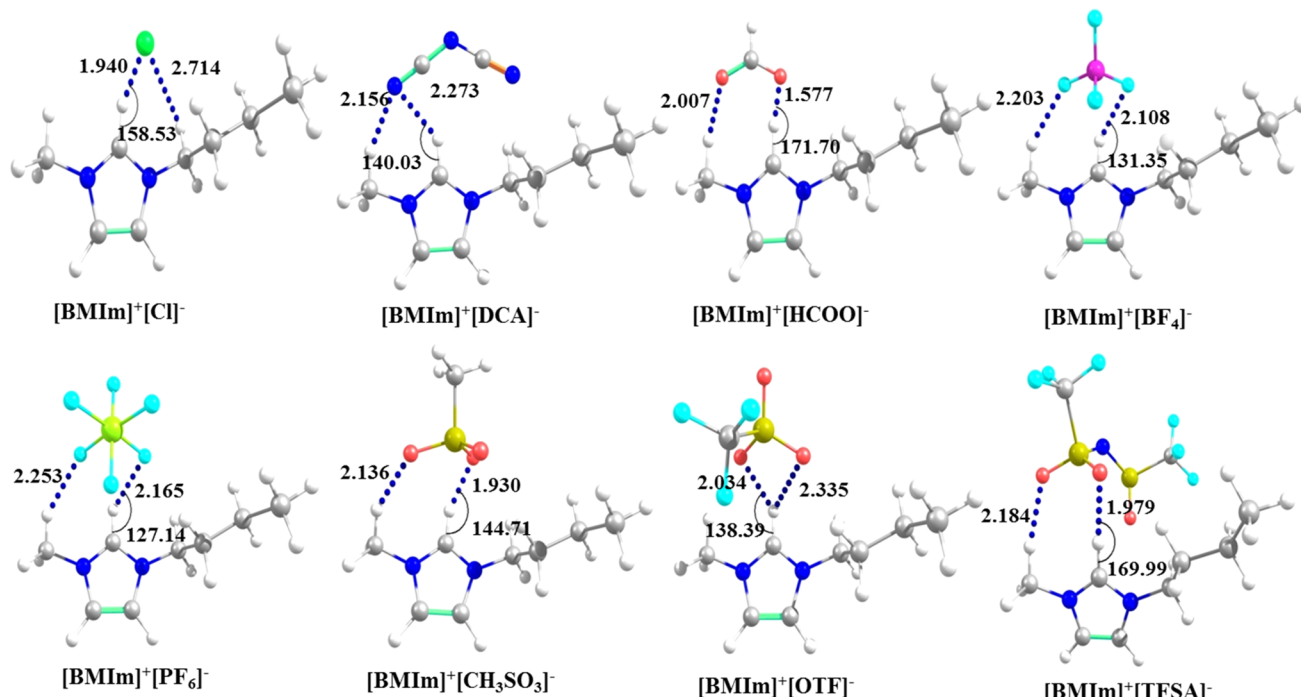


Figure 1. Optimized structures of ILs computed at the PBE/6-311++G** level along with the cation–anion distances (in Å) and angles (in degree).

exists in the case of $[\text{HMIm}]^+[\text{Cl}]^-$ with Ag where a chemisorbed $[\text{HMIm}]^+[\text{Cl}]^-$ is identified (i.e., Ag–Cl bond).⁵³ These studies clearly reveal that there is no clear evidence to understand the adsorption mechanism of ILs on surfaces and the nature of bonding between them. The framework of the present study will thus give valuable complementary information to understand the uncovered mechanism at the molecular level with different BMIm-based ILs. Indeed, we have modeled ionic liquid electrolytes in interaction with the Au(111) surface to mimic the electrode–electrolyte interface using first-principles computation approaches. We have selected both hydrophilic (i.e., $[\text{BMIm}]^+$ with $[\text{Cl}]^-$, $[\text{DCA}]^-$, and $[\text{HCOO}]^-$) and hydrophobic (i.e., $[\text{BMIm}]^+[\text{X}]^-$, where $\text{X} = \text{BF}_4^-$, PF_6^- , CH_3SO_3^- , OTF, and TFSA) ionic liquids. First, we treated these ILs in gas phase. Then, we considered ILs@Au(111) to shed light on the adsorption mechanism, structural orientation, and bonding of ILs on the gold surface. We found that gold surface and IL interactions are mainly dominated by electrostatics and vdWs type of forces. Thus, the inclusion of dispersion correction (DFT-D3) is important to describe and understand the dispersive role during the molecular adsorption at the solid–liquid interface. We also show that three different modes of attractions are possible during the adsorption: (i) anion-induced cation adsorption on the hydrophilic ILs@Au(111) surface, (ii) stabilization of cation through long-range dispersive interactions, followed by adsorption of the anion interacting with the cation in hydrophobic ILs, and (iii) adsorption of the alkyl group depending on the nature of anion and ion-pair interactions. These findings will be established and discussed in this article.

2. RESULTS AND DISCUSSION

2.1. Equilibrium Geometries and Energetics of Ionic liquids (ILs) in Gas Phase

We considered both hydrophobic

and hydrophilic ionic liquids. These ILs are composed of the $[\text{BMIm}]^+$ cation with various X^- anions (where $\text{X} = \text{Cl}$, $(\text{CN})_2\text{N}$ (DCA), HCOO , BF_4^- , PF_6^- , CH_3SO_3^- , CF_3SO_3^- (OTF), and $(\text{CF}_3\text{SO}_2)_2\text{N}$ (TFSA or NTf₂)). They are denoted $[\text{BMIm}]^+[\text{X}]^-$. All of these ILs are hydrophobic, except for $\text{X} = \text{Cl}$, DCA, and HCOO. Figure 1 shows the optimized geometries of all of these ILs as computed at the PBE/6-311++G** level of theory. As can be seen in this figure, all anions interact through hydrogen bond (H-bond) with the carbon atom present between two N atoms of the imidazole (Im) subunit of BMIm⁺ (i.e., C₂ position in the ring). Indeed, we identified these C₂–H…Cl, C₂–H…N, C₂–H…O, C₂–H…F, and C₂–H…O H-bonds for the complexes involving the Cl⁻, DCA⁻, HCOO⁻, BF₄⁻, and TFSA⁻ anions, respectively. It is interesting to note that OTF⁻ forms a three-centered H-bond with the C₂–H group.

Table 1 lists the interionic distances, defined here by the H-bond involving the carbon at the C₂ position, and the basis set

Table 1. Calculated BSSE-Corrected Binding Energies (BEs, in kcal/mol) of Various ILs ($[\text{BMIm}]^+[\text{X}]^-$) at the PBE/6-311++G** Level^a

$[\text{BMIm}]^+[\text{X}]^-$ where $\text{X} =$	BEs		
	PBE	PBE+D3 ^b	distance (Å)
Cl	-95.29	-96.96	1.94
DCA = $(\text{CN})_2\text{N}$	-81.90	-85.03	2.27
HCOO	-101.74	-103.80	1.58
BF_4^-	-85.55	-89.21	2.10
PF_6^-	-79.72	-84.30	2.16
CH_3SO_3^-	-93.30	-97.80	1.93
OTF = CF_3SO_3^-	-82.49	-87.25	2.03
TFSA = $(\text{CF}_3\text{SO}_2)_2\text{N}$	-77.24	-83.65	1.98

^aInterionic distances (in Å) are also provided. ^bWith dispersion using optimized geometries from the PBE/6-311++G** method.

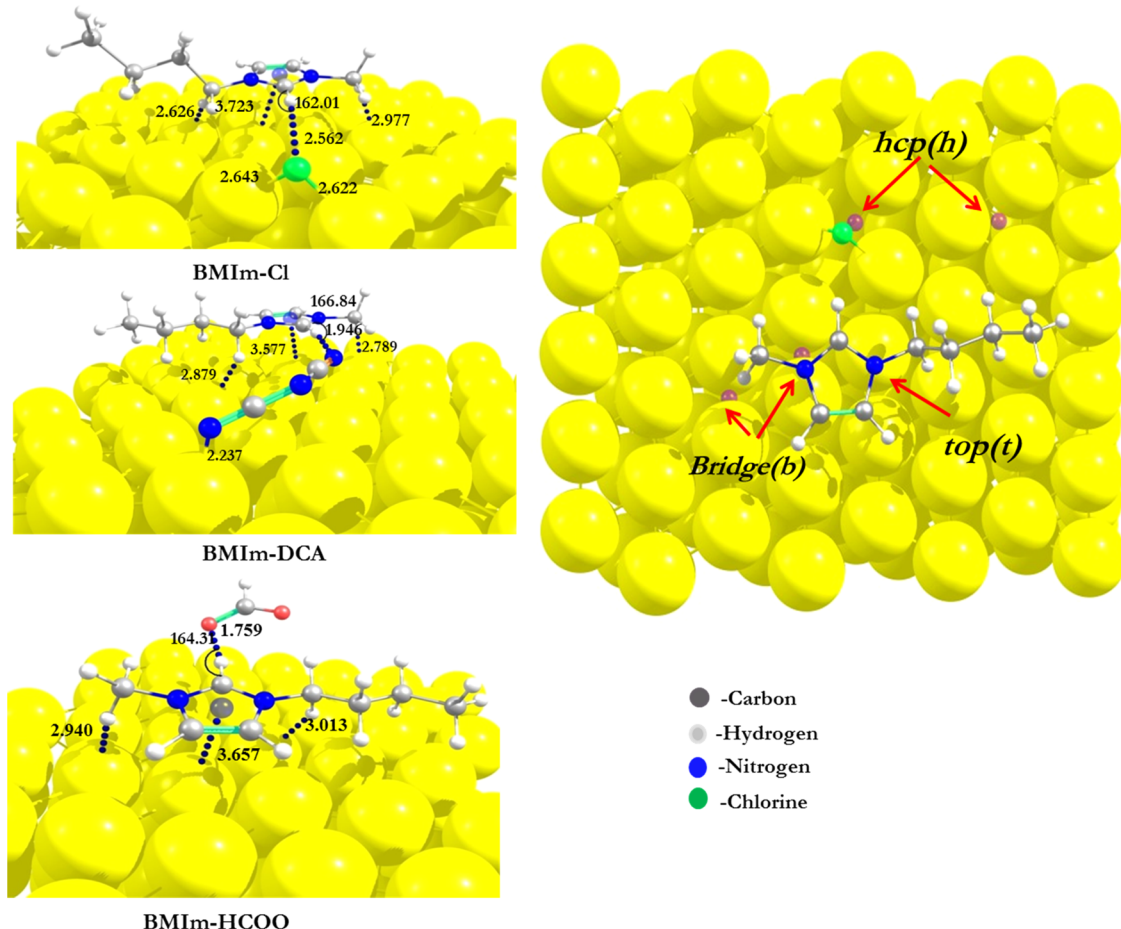


Figure 2. Optimized geometrical structures, as computed at the PBE+D3/TZVP level of theory, of various hydrophilic ILs@Au(111) surfaces and nearest interacting distances (in Å) between ILs and the Au(111) surface. In bottom, we show the top (t), bridge (b), and hexagonal close-packed (hcp) hollow (h) sites of the different adsorption sites of $[\text{BMIm}]^+[\text{Cl}]^-$ on the Au(111) surface.

superposition error (BSSE)-corrected binding energies (BEs) of $[\text{BMIm}]^+[\text{X}]^-$ as computed at the PBE/6-311++G** level. The calculated distances vary in the range 1.57–2.27 Å. The shortest one is observed between $[\text{BMIm}]^+$ and $[\text{HCOO}]^-$ species. For BEs, we computed values in the –77.2 to –101.7 kcal/mol energy range. These values are relatively large because of the ionic nature of the bonding within ILs. This is due to the formation of double H-bonds between the anions and the $[\text{BMIm}]^+$ cation. The largest BE is for $[\text{BMIm}]^+[\text{HCOO}]^-$ in accordance with the shortest intermonomer distance computed for this IL. The weakest interaction energies are observed for $[\text{BMIm}]^+$ interacting with $[\text{PF}_6]^-$ and $[\text{TFSA}]^-$ ILs. This is due to the highly hydrophobic nature of the perfluoro moiety that may reduce the electrostatic interactions. In Table 1, we provide also the BSSE-corrected BEs including dispersion correction (i.e., Perdew, Burke, and Ernzerhof (PBE)+D3). This table shows that the contribution of D3 correction to BEs is not negligible and amounts to ~2–6 kcal/mol. The D3-corrected BEs are larger (in absolute value).

2.2. ILs@Au(111) Surface. 2.2.1. Hydrophilic IL Adsorption on the Au(111) Surface. To study the nature of interactions between the gold surface and ILs, we performed periodic computations. First, the optimized gas-phase geometries of $[\text{BMIm}]^+[\text{X}]^-$ (where X = Cl, DCA, and HCOO) ILs were used as the starting point for these computations. Dispersion correction terms have been incorporated during the bulk-phase optimization. The bulk-phase geometries of

Au(111) and hydrophilic ILs are shown in Figure 2 along with the important distances. This figure shows that the $[\text{BMIm}]^+$ cation has its imidazole ring parallel to the surface, where distances of ~3.577–3.723 Å are computed between the imidazole entity and gold surface. These distances are in good agreement with vdW type of interactions between these hydrophilic ILs and the Au(111) surface via the $\pi-\pi$ stacking prototype model. In addition, we observe anchor-assisted H-bonds between the alkyl chain and Au atom ($\text{C}_{\text{alkyl}}-\text{H}\cdots\text{Au}(\text{s})$) as those found for imidazole attached to Au_n clusters. Indeed, we previously established that these anchor-assisted H-bonds significantly enhance the stability of such complexes.⁵⁴ Figure 2 shows also that the Cl^- and DCA^- anions are strongly bonded with the Au surface where they form bonds with Au atoms except the HCOO^- anion. After the adsorption of ILs at the gold surface, the ion-pair interactions are disrupted because of the covalent and noncovalent interactions of ions with the surface. Particularly, Cl^- adsorbs on a bridge site of the Au surface, whereas DCA^- is bonded with Au on the top site via the nitrogen atoms, where the HCOO^- anion is simultaneously interacting with the surface and the cation through H-bond (i.e., C_2-H). The calculated ion-pair H-bond distances show that there is a strong interaction of HCOO^- (1.759 Å) and DCA^- (1.946 Å) anions at the interface, whereas the same distance for $[\text{BMIm}]^+[\text{Cl}]^-$ is distinctly longer (2.562 Å) because of the formation of the Au–Cl bond at a perfect site in the interface. The significant changes in the ion pairs may

Table 2. Calculated Adsorption Energies (E_{ads} , in kcal/mol) and Distances (in Å) between the Cation and Anion of the ILs@Au(111) Surface ($[\text{BMIm}]^+[\text{X}]^-@\text{Au}(111)$) Using PBE and PBE+D3 Methods^a

$[\text{BMIm}]^+[\text{X}]^-$ where $\text{X} =$	PBE/TZVP	PBE+D3/TZVP	PBE+D3/TZV2P ^b	PBE+D3/TZVP	PBE+D3/6-311++G**
	E_{ads}	E_{ads}	E_{ads}	D_{ads}	D_{gp}
Cl	-23.99	-81.78	-71.23	2.56	1.94
DCA = $(\text{CN})_2\text{N}$	-13.08	-78.06	-70.62	1.95	2.27
HCOO	5.04	-19.26	-22.38	1.76	1.57
BF_4^-	14.42	-41.49	-24.40	2.20	2.10
PF_6^-	7.11	-46.57	-27.82	2.01	2.16
CH_3SO_3^-	2.87	-8.41	-17.32	1.92	1.93
OTF = CF_3SO_3^-	6.60	-40.98	-27.38	2.27	2.03
TFSA = $(\text{CF}_3\text{SO}_2)_2\text{N}$	133.13	-28.58	-38.38	2.11	1.97

^aThe PBE+D3 computations were done using the PBE/TZVP optimized geometry. D_{gp} and D_{ads} (in Å) are the intermonomer distances between the anion and the cation for $[\text{BMIm}]^+[\text{X}]^-$ in gas phase and when the same moiety is adsorbed at the Au(111) surface, respectively. ^b E_{ads} calculated from PBE+D3/TZVP geometries for the TZV2P basis set (consider only for IL).

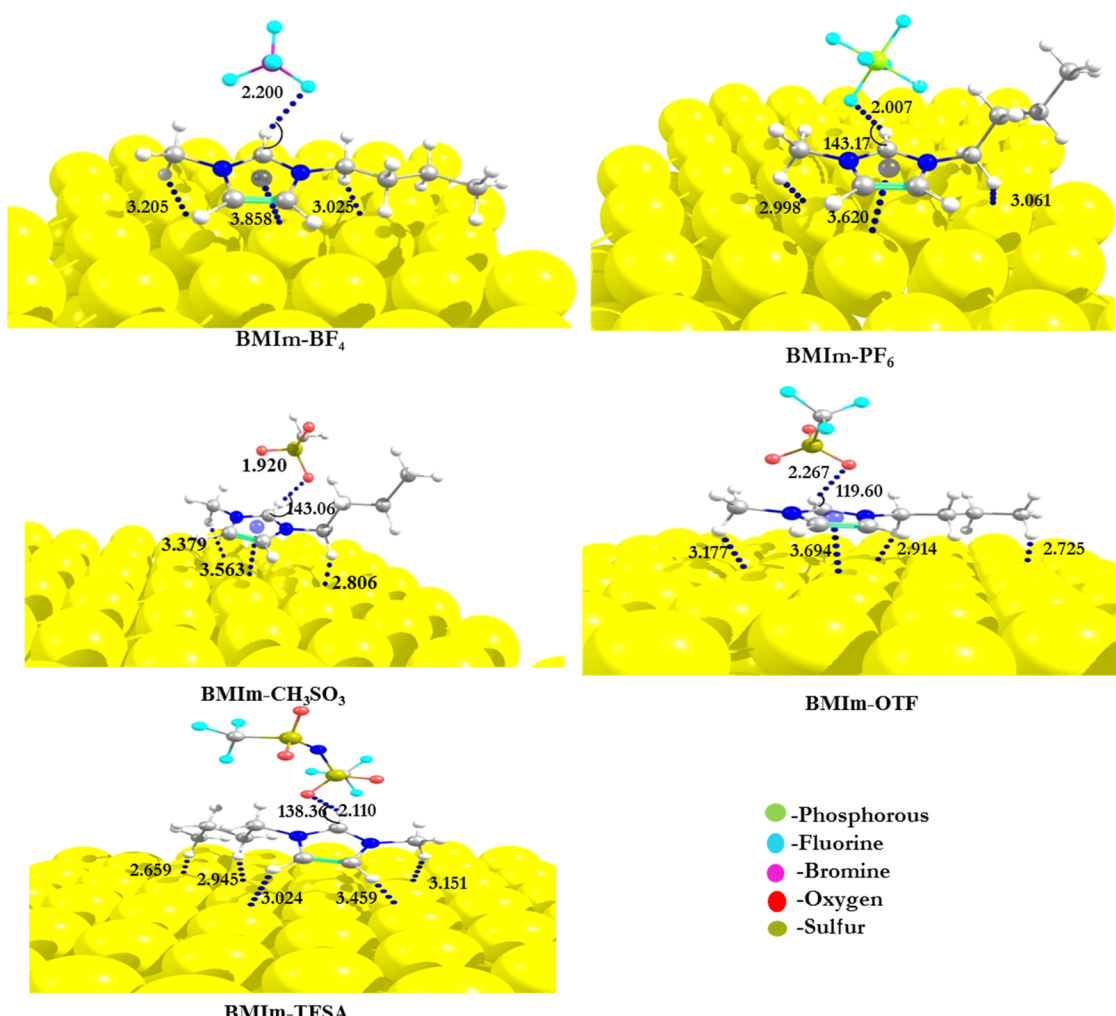


Figure 3. Optimized equilibrium structures, as computed at the PBE+D3/TZVP level of theory, of various hydrophobic ILs on the Au(111) surface. We give also the nearest interacting distances (in Å) and angles (in degree) between ILs and the Au(111) surface.

happen from the bond formation between the Au(111) surface with Cl^- and $\text{N}(\text{DCA})^-$ anions. The interaction strength can be calculated from the calculated adsorption energies.

Table 2 gives the adsorption energies (E_{ads}) of these ILs on Au(111) using the TZVP basis set. As can be seen, there are large deviations between the E_{ads} values computed with and without inclusion of dispersion corrections, where ILs are optimized at the respective level of theory. This clearly reveals

that the dispersion interaction plays a crucial role in the adsorption of these ILs on the Au(111) surface. Because of the vdW type of interaction in these adsorptions, the PBE+D3 E_{ads} values are clearly viewed to be more accurate, and in the following, we will refer to this set of data.

We computed two slightly different Au–Cl distances (of ~2.64 and 2.62 Å) for $[\text{BMIm}]^+[\text{Cl}]^-@\text{Au}(111)$ (Figure 2). For $[\text{BMIm}]^+[\text{DCA}]^-@\text{Au}(111)$, a shorter Au–N distance of

2.237 Å is obtained, the other Au–N distances being slightly longer. The corresponding E_{ads} values of these hydrophilic ILs are –81.78 and –78.06 kcal/mol for Cl and DCA, respectively (Table 2). The calculated E_{ads} at TZV2P (using TZVP geometry) for the same ILs are –71.23 and –70.62 kcal/mol, respectively, that is, around 10 kcal/mol smaller. It is found that the DFT+D3 BE of $[\text{BMIm}]^+[\text{HCOO}]^-$ at the surface is very low when compared to that of other hydrophilic ILs, the BE is ~–22 kcal/mol using the PBE+D3/TZV2P method. This clearly reveals that the binding strength of ILs depends on the nature of the anion and binding mode of ILs, either dispersive or covalent bond.

2.2.2. Hydrophobic IL Adsorption on the Au(111) Surface.

Figure 3 shows the optimized structures of various hydrophobic ILs on Au(111) along with some respective interacting distances. We considered $[\text{BMIm}]^+[\text{X}]^-$ ILs, where X = BF₄[–], PF₆[–], CH₃SO₃[–], OTF, and TFSA. This figure shows that $[\text{BMIm}]^+$ mostly lies parallel to the gold surface and is stabilized by π – π stacking interactions except for $[\text{BMIm}]^+[\text{TFSA}]^-$. Indeed, $[\text{BMIm}]^+[\text{TFSA}]^-$ exhibits a strong interaction between perfluoro derivatives of the TFSA anion and the C₂ position of $[\text{BMIm}]^+$ through H-bond (~2.1 Å). Moreover, our computations show that the alkyl group of the cation is adsorbed on the Au surface except PF₆[–] and CH₃SO₃[–]. The calculated distances between the Au(111) surface and the center of the $[\text{BMIm}]^+$ cation are in the ~3.56–3.80 Å range. In addition to above-mentioned interactions, anchor-assisted H-bonds also stabilize the hydrophobic ILs at the Au(111) surface. The calculated C_{alkyl}–H...Au interacting distances vary from ~2.8 to 3.2 Å, depending on the anion.

In contrast to the case of $[\text{BMIm}]^+[\text{X}]^-$ (where X = Cl, DCA) hydrophobic ILs, Figure 3 shows that the interaction of the Au(111) surface occurs only with the $[\text{BMIm}]^+$ cation because no bonding is observed between the anions and gold atoms. Instead, these hydrophobic anions form a complex with the adsorbed $[\text{BMIm}]^+$ cation, i.e., localized above the cation entity. The H-bonding distances between the anion and the cation within these ILs vary from ~1.759 to 2.267 Å after the adsorption.

Table 2 provides the calculated adsorption energies (E_{ads}) of hydrophobic ILs with and without considering dispersion correction. This table shows that the E_{ads} values of these ILs as computed with the PBE/TZVP method are wrongly positive, contrary to those of the hydrophilic ILs. Instead, negative E_{ads} values are computed when the D3 correction is included. This is due to the dispersive interaction, which dominates the $[\text{BMIm}]^+$ and Au(111) surface interaction. This observation is in line with the experimental studies of ILs at Au(111) surfaces by in situ STM.⁴²

Even though the same cation is considered in these hydrophobic ILs, different E_{ads} values are computed. At the DFT+D3 level, we estimate E_{ads} values of –46.57, –41.49, –8.41, –40.98, and –28.58 kcal/mol for $[\text{BMIm}]^+[\text{X}]^-$, where X is PF₆[–], BF₄[–], CH₃SO₃[–], OTF (CF₃SO₃[–]), and TFSA ((CF₃SO₂)₂N), respectively (Table 2). These E_{ads} values are distinctly lower (by at least 50%) from those derived for $[\text{BMIm}]^+[\text{Cl}]^-@ \text{Au}(111)$ and for $[\text{BMIm}]^+[\text{DCA}]^-@ \text{Au}(111)$.

To elucidate the role of the anion in the Au(111)– $[\text{BMIm}]^+$ interaction, we list in Table 3 the adsorption energies of the $[\text{BMIm}]^+$ cation alone with respect to the anion. These adsorption energies are computed using the following formula

Table 3. Different Adsorption Sites Observed from Optimized Geometries of the $[\text{BMIm}]^+[\text{X}]^-@ \text{Au}(111)$ Surface^a

$[\text{BMIm}]^+[\text{X}]^-$ where X=	N-R_1^{b}	N-R_2^{c}	E_{ads}	anion sites
Cl	hcp	bridge	–93.9	bridge
DCA = (CN) ₂ N	bridge	bridge	–95.9	top
HCOO	hcp	hcp	–106.3	bridge
BF ₄	top	top	–105.9	
PF ₆	bridge	bridge	–94.6	
CH ₃ SO ₃	bridge	hcp	–99.6	
OTF = CF ₃ SO ₃	bridge	bridge	–99.8	
TFSA = (CF ₃ SO ₂)N	bridge	hcp	–99.6	

^aThese sites correspond to top (t), bridge (b), and hcp (h) as described in the text. E_{ads} (in kcal/mol) is the adsorption energy of the $[\text{BMIm}]^+$ cation on Au(111) with respect to different anions as computed at the PBE+D3/TZVP level. Note that only Cl[–] and DCA[–] anions were adsorbed on the Au(111) surface. The other anions were adsorbed on the cation and not on the Au(111) surface. ^bN-R₁ represents the methyl. ^cN-R₂ represents the butyl group in $[\text{BMIm}]^+$.

$$E_{\text{ads}}(\text{cation}) = E_{\text{BMIm}@\text{Au}(111)} - (E_{\text{Au}(111)} + E_{\text{BMIm}}) \quad (1)$$

where $E_{\text{BMIm}@\text{Au}(111)}$, $E_{\text{Au}(111)}$, and E_{BMIm} energies were obtained from single point computations at the PBE(+D3)/TZVP optimized geometries.

The calculated energies reveal that the cationic adsorption significantly dominates over that of the anion because these energies are as large as –94.0 to –106.0 kcal/mol, i.e., at least twice of those given in Table 2 for the hydrophobic ILs. Moreover, this table shows that there are three different ranges of E_{ads} due to alkyl group adsorption on the Au(111) surface. Indeed, the contribution of the alkyl group is significant enough to alter the stability of the ILs on surface binding. This depends on the number of CH₂ subunits adsorbed on the Au(111) surface.

2.2.3. Adsorption-Induced Effects of $[\text{BMIm}]^+[\text{X}]^-$ ILs on Au(111). Close examination of the optimized geometries of ILs at gas and solid–liquid phases reveals that there are slight structural changes of IL subunits upon adsorption at the Au(111) surface. However, the intermonomer distances between the anion and the cation are changed. Indeed, the intermonomer distances between the anion and the cation significantly deviate from the gas phase to the solid surface interface for the hydrophilic ILs (Cl, DCA, and HCOO) and some hydrophobic ILs (OTF and TFSA), as shown in Table 2. The large deviations in hydrophilic IL interactions are mainly due to the covalent bond formation between the anion and the surface. Thus, these effects may affect the electrostatic behavior of ILs at the gold surface, which favors the charge transfer process.

The stability depends on the nature of the adsorption sites of the anion, cation, and alkyl groups and on the charge transfer phenomena between these complexes. The adsorption behavior of the eight different ILs and their electron density profiles on the Au(111) surface are shown in Figures 4 and 5. The cationic part of IL interacts through the Au(111) surface via vdWs interactions from the $[\text{BMIm}]^+$ cation and anchor-assisted H-bond from its alkyl group, whereas for anions, the interaction depends on their hydrophilic/hydrophobic character. Both hydrophilic anions are here directly bonded with the top or bridge site of the Au(111) surface. Previously, we have reported that for Im@Au(111) the interaction sites of Im with Au(111) may reflect the bonding nature of the complex.⁵⁵

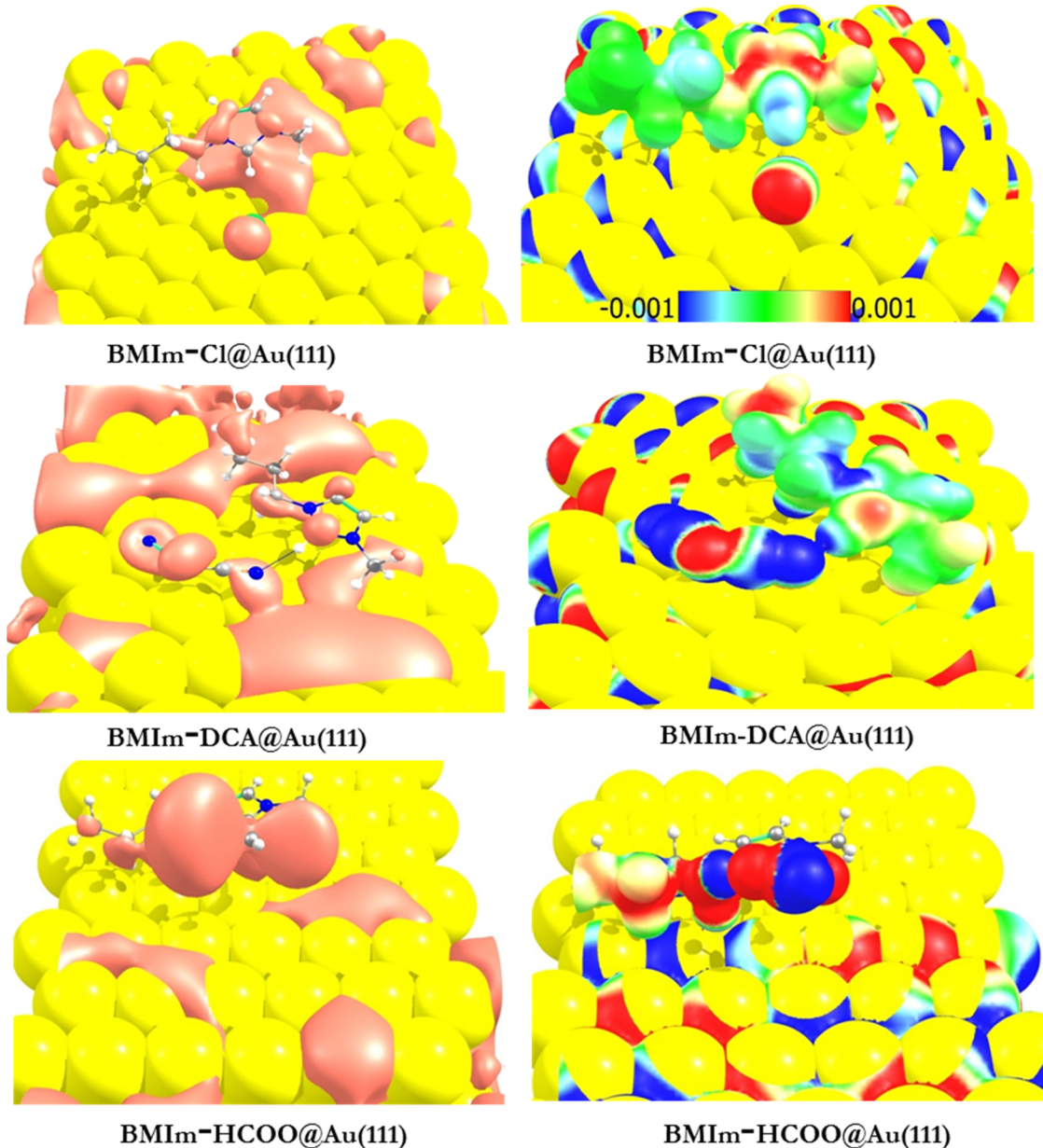


Figure 4. Electron density surface (isosurface value of 0.001 au) of various hydrophilic ILs@Au(111) surfaces.

Indeed, we found that N(Im) strongly binds with the top site of the Au(111) surface. Similarly, we found that there are different sites on Au(111) available for binding, and respective binding sites are provided in Table 3 for all ILs@Au(111). The selective adsorption sites of cation–anion are shown in Figure 2. To predict the effect of the anion on the binding character, we have also calculated E_{ads} for $[\text{BMIm}]^+$ at the Au(111) surface for various anions optimized as given by eq 1. Here, we found that anions play a vital role in the selective adsorption, site selectivity, and reactivity with the surface. This will be reflected in the BEs of the complexes.

Table 3 shows the specific adsorption sites of ILs at the gold surface. This table reveals that the cation (N atoms) is mostly attracted by the bridge site except $[\text{BMIm}]^+$ with $[\text{BF}_4]^-$ (top) and $[\text{HCOO}]^-$ (hcp), whereas anions are attracted by different sites, depending on the size of the anion. For example, hydrophilic ILs, with $[\text{Cl}]^-$ and $[\text{DCA}]^-$ anions, adsorb at the bridge (b) and top (t) sites, respectively. These anions are not

interacting at the hcp (h) site. The respective N atoms in the cation for Cl interact with (h, b) and DCA in (b, b) sites. The other mode of interaction at the interface concerns alkyl chain adsorption on the Au surface. There are three different kinds of interactions, that is, C–H…Au, $\text{CH}_2\cdots\text{Au}$, and $\text{CH}_3\cdots\text{Au}$. All of these interactions increase E_{ads} and also affect the local charge density. This will enhance the charge transfer process at electrode–electrolyte interfacial sites.

2.3. Charge Transfer, Electron Density and Molecular Orbital Analyses. Adsorption and desorption mechanisms play a vital role in the charge transfer phenomenon of the electrode–electrolyte interface materials, as shown by numerous experimental and theoretical studies.^{56–59} Indeed, the nature of ILs is of great importance in the charge transfer process through the electrochemical window.^{56,57} These reports state that the adsorption mechanism of anions and cations on a metal surface is essential to understand the charge transfer mechanism and specific adsorption sites. For instance,

most of previous works varied the potential ranges, which cause the orientation of the ILs at the charged surfaces, observed by STM and atomic force microscopy (AFM), followed by the formation of EDL of ILs adsorbed at solid surfaces.⁵⁸ The *in situ* STM study of a potential-dependent surface showed restructuring and electrochemical annealing of the Au(111) electrode in the 1-butyl-3-methylimidazolium tetrafluoroborate [BMIm-BF₄] ionic liquid. Also, this work found that the long-range surface restructuring phenomenon is observed because of the partial charge transfer to the weakly adsorbed [BMIm]⁺ and synergistic effect of the counter anion BF₄⁻, which reduces the metal–metal cohesive energy.⁵⁹

In the present work, we identified relatively strong interactions between [BMIm]⁺ and the Au(111) surface. Thus, the electrostatic surface defects may be enhanced and can easily attract hydrophilic anions through charge transfer phenomena. Consequently, ILs form an adlayer on the Au(111) surface as observed in the recent *in situ* STM studies of ILs at the Au(111) surface.⁴⁰ These interactions induce charge transfer processes between the gold electrode surface and ILs, which are of great importance for the electrochemical applications discussed above. Moreover, such an environment can affect the reactivity of the gold surface.

We have performed electron density analysis (EDA) for a Au(111) neutral surface model. For instance, we performed EDA by using the Perdew, Burke, and Ernzerhof (PBE) exchange–correlation functional as implemented in the C2PK code. The effects of core electrons and nuclei were treated with Geodecker–Teter–Hutter (GTH) pseudopotentials. For representing all valence electrons, we used the cutoff value 400 Ry and set triple- ζ double-polarized basis sets. We have generated a cube density file from the optimized coordinates (at PBE+D3/TZVP) to study the charge distribution on the surface and ILs. Moreover, we used optimized coordinates to perform the energy calculations. The EDA pictures of adsorption of hydrophilic and hydrophobic ILs on the gold surface are shown in Figures 4 and 5, respectively. The red isosurface represents the positive charge accumulation, and light yellow and blue end shows the negative charge accumulations on the atoms at the surface. The adsorption of [BMIm]^{+[Cl]⁻ on the Au(111) surface was confirmed by the electron density picture. The red color of ILs shows the positive charge on the imidazolium nitrogen and the Cl atom adsorbed on the gold surface. The green and light yellow color indicates the neutral charge accumulations of the alkyl chain and methyl groups connected to the imidazolium rings, respectively.}

Table 3 shows the selective adsorption sites of various anions containing [BMIm]⁺ ILs, and corresponding E_{ads} values with respect to different anions are shown in Figure 6. Our study clearly reveals that whenever [BMIm]⁺ adsorbs at the bridge site the calculated E_{ads} is smaller when compared to E_{ads} for top and hcp adsorption sites. It is interesting to note that [BMIm]⁺ of HCOO⁻ and BF₄⁻ anions were strongly adsorbed when compare to the other anions. This reveals that the N-based moiety prefers to stay at the top/hcp sites of the gold surface. An earlier report on Im@Au(111) revealed that N(Im) always prefers to interact with the top site of the gold surface.⁵⁵ This is also confirmed by the analysis of the electron density of [BMIm]⁺ adsorbed on Au(111) (Figure 4). Indeed, this figure shows that the bridge site selectivity dominates over that for the other sites. The density pictures of adsorption of all ILs exhibit the same features except for ILs containing BF₄⁻

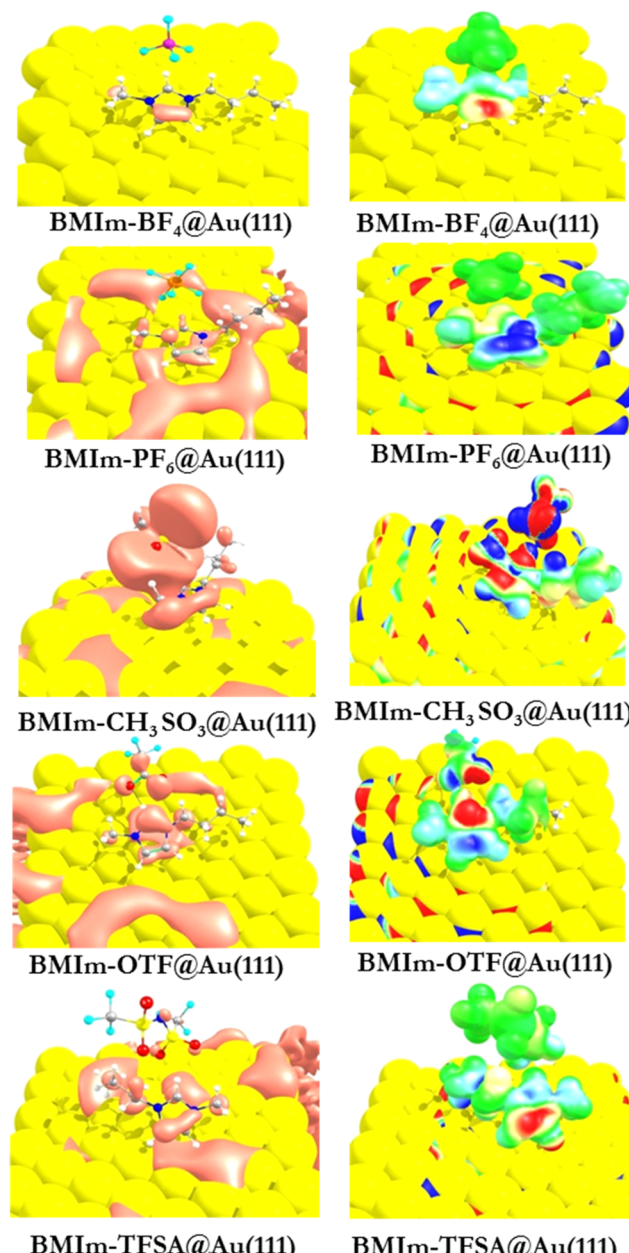


Figure 5. Electron density surface (left: isosurface value of 0.001 au; right: mapped sphere for 0.001 au) of various hydrophobic ILs@Au(111) surfaces.

and HCOO⁻ anions. The spin density plot of [BMIm]^{+[Cl]⁻ at the gas and solid–liquid interface is shown in Figure 7. This confirms the charge distribution of anions and cations at the gold surface, which favors the electrostatic behavior.}

Table 4 provides the Mulliken, Hirshfeld, and Löwdin charge analyses of gas-phase ILs of interest in the present study and ILs adsorbed at the Au(111) surface. This table shows that all three analyses provide the same trend evolution for the charge transfer from the gas phase into the solid–liquid interface. However, Löwdin charges significantly enhance the electrostatic behavior compared with the other two methods. Indeed, the computed potential difference values between [BMIm]^{+[Cl]⁻ and the Au(111) surface using Mulliken, Hirshfeld, and Löwdin approaches are ~0.62, ~1.02, and ~2.11 au, respectively. This enhancement is related to the}

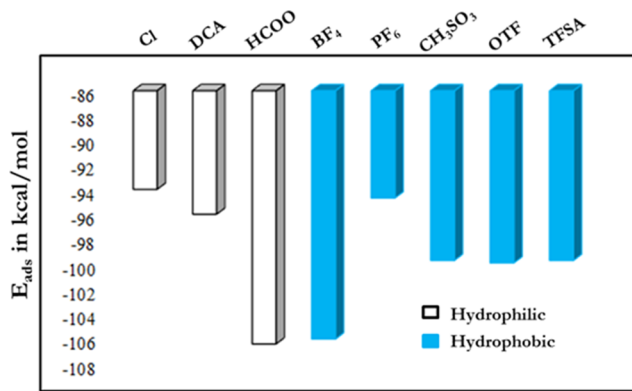


Figure 6. Adsorption energy of $[\text{BMIm}]^+$ at the Au(111) surface with respect to the different anions (i.e., hydrophilic and hydrophobic ILs).

nature of interactions between ILs and the interface. Indeed, anions weakly adsorbed at the surface exhibit fewer enhancements, whereas covalently bonded anions have the opposite behavior. For instance, DCA^- presents the same behavior as that of Cl^- and the HCOO anion does not.

In the following discussions, we will use Löwdin charges (shown in bold characters in Table 4). The comparison of partial charges of the IL ion pairs in the gas phase and at the solid–liquid interface shows that there is a significant enhancement in the partial atomic charge on the ion pair upon adsorption. For hydrophilic ILs on the gold surface, the atomic charges are, for instance, 3 times larger than those in the gas phase (except for the HCOO anion). For hydrophobic ILs, charges are varied from ~1.5 to 2 times. These changes are very significant and modify the reactivity of the surface at the microscopic scale. They can promote the charge transfer in the Au(111)–IL composite and the binding strength of ILs at this interface through various covalent and noncovalent interactions such as vdWs, electrostatic, and dipole-induced dipole interactions. We found that there is a significant charge transfer between the gold surface and hydrophilic ILs at this interface. Indeed, one can see a relatively large positive charge localized on Cl^- and $\text{N}(\text{DCA})^-$ in the Löwdin scheme after adsorption of Cl^- and DCA^- on the Au(111) surface. The calculated partial charges for these two anions at the gold surface are 2.11 and 1.82 au, respectively.

It is interesting to note that after adsorption of ILs at Au(111) the Au surface potential becomes negative for all complexes and particularly charge transfer is significant in hydrophilic ILs. The respective partial charges on the Au surface are as follows: for Cl , -2.11; for DCA , -1.82; for HCOO , -0.16; for BF_4 , -0.56; for PF_6 , -0.52; for CH_3SO_3 , -0.50; for OTF , -0.66; and for TFSA , -0.34. The HCOO anion-containing gold surface has very less negative charges than those of the surfaces with the other anions. This is due to the strong electrostatic interaction between IL ion pairs and the Au(111) surface. For instance, the adsorbed cation can induce stronger binding of the cation compared with the anion. This unusual effect can significantly enhance the Coulombic electrostatic interaction between ILs and the surface. Note that AFM studies on ILs at the Au(111) surface revealed a similar effect with EDL formation at the electrode–electrolyte interface.²³ For the $[\text{BMIm}]^+[\text{X}]^-@\text{Au}(111)$ surface, the order of magnitude of the distribution of charge observed at the gold surface is $\text{Cl}^- > \text{DCA}^- > \text{OTF}^- > \text{BF}_4^- > \text{PF}_6^- > \text{CH}_3\text{SO}_3^- > \text{TFSA}^- > \text{HCOO}^-$. This may provide an

explanation for the nature of the interactions and of the adsorption sites. Therefore, the charge transfer process can be influenced and guide the IL interaction with the Au surface. Thus, our study should be helpful to select the suitable composite material for the energy storage and electrochemical applications.

3. CONCLUSIONS

The adsorption of hydrophilic and hydrophobic ILs such as $[\text{BMIm}]^+[\text{X}]^-$ [where $\text{X} = \text{Cl}$, DCA , HCOO , BF_4 , PF_6 , CH_3SO_3 , OTF , and TFSA] on the Au(111) surface is studied by DFT-based PBE and PBE+D3 methods. Our study clearly reveals that dispersive interaction plays a dominant role in the stability of the ILs@Au(111) surface, which is confirmed by our DFT+D3 approach. It is found from our calculations that there are several modes of attractions possible during the adsorption: (i) anion-induced cation adsorption on the hydrophilic ILs@Au(111) surface, (ii) whereas in the hydrophobic case, the cation first stabilizes through long-range dispersive interaction, followed by adsorption of the anion and (iii) adsorption of the alkyl group depending on the nature of the anion and ion-pair interactions. Thus, hydrophilic anions of ILs tightly adsorbed on the gold surface through covalent bonds in addition to this, anions and cations were stabilized through H-bonded interactions. These three different kinds of adsorption are also reflected in the E_{ads} . In addition, our work shows that adsorption of the alkyl chain of $[\text{BMIm}]^+$ on the gold surface can enhance the stability and charge transfer process through anchor-assisted H-bond except in the case of the $[\text{BMIm}]^+$ cation with $[\text{PF}_6]^-$ and $[\text{CH}_3\text{SO}_3]^-$ anions. Our studies reveal that the unusual effect of surface charges can induce the electrostatic interaction between the ion pair and Au(111) surface.

The present investigations of the structure and dynamics of various ILs at the Au(111) surface can be helpful to understand the adsorption mechanism at the microscopic level and charge transfer between electrode and electrolyte materials for energy harvesting and catalysis applications. Our studies should also be useful for the selection of ILs at the solid–liquid interface for energy storage applications.

4. COMPUTATIONAL DETAILS

In this work, we performed computations of isolated ILs and of ILs in interaction with the gold surface. These electronic structure computations are carried out using Perdew–Burke–Ernzerhof (PBE) generalized gradient approximation density functional theory (DFT) to treat exchange–correlation⁶⁰ with and without considering Grimme's latest version of empirical correction term (DFT-D3) to study the effect of dispersion correction.^{61–63} Indeed, dispersion correction should help in properly describing the interaction in solid–liquid and solid–gas interface systems, especially for composite materials composed of organic molecules and metal surfaces.⁵⁵

For ILs, computations consisted of geometry optimizations without constraints at the PBE(+D3) level, followed by frequency calculations to confirm the minimum nature of the conformations. All electronic structure calculations were performed using the GAUSSIAN 16 and GaussView 6.0 software packages.⁶⁴ The atoms were described with the 6-311++G** basis set.⁶⁵ The binding energies (BEs) of the IL complexes are calculated within the supramolecular approach and corrected for the basis set superposition error (BSSE)

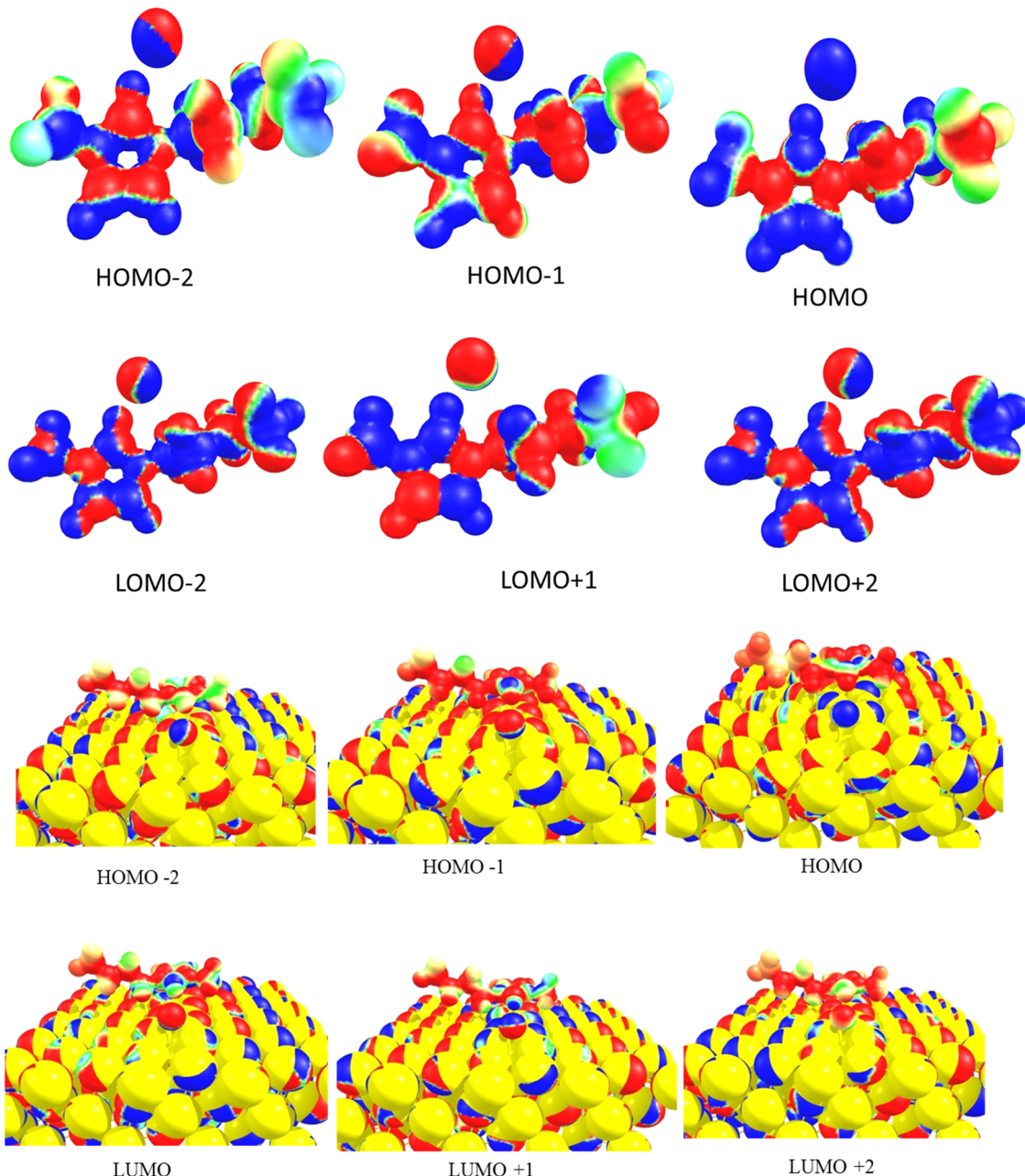


Figure 7. Spin density plots of $[{\text{BMIm}}^+] \text{Cl}^-$ @gas and solid–liquid interface. The blue and red colors represent the positive and negative spin densities, respectively.

employing the counterpoise (CP) procedure of Boys and Bernardi⁶⁶

$$\text{BE(IL)} = (E_{\text{IL}} - (E_{\text{anion}} + E_{\text{cation}})) \quad (2)$$

where E_{IL} , E_{anion} , and E_{cation} are the total energies of the IL, anion, and cation as computed in the full basis set of the IL complex.

For the computations of ILs interacting with the gold surface, we used the CP2K/Quickstep code with periodic DFT calculations.⁶⁷ A hybrid basis set formalism known as a Gaussian and Plane Wave⁶⁸ (GPW) is implemented in CP2K, where the Kohn–Sham orbitals are expanded in terms of contracted Gaussian type orbitals, whereas an auxiliary plane wave basis set is used to expand the electronic charge density. Indeed, valence electron density and pseudopotentials are

expressed by a mixed GPW basis set scheme.⁶⁹ All atoms, except Au, were represented by the optimized MOLOPT-TZVP basis set,⁷⁰ whereas we used the DZVP-MOLOPT-SR-GTH (SR denotes a shorter range) basis set for Au atoms. A plane wave cutoff (of 400 Ry) was included. Orbital transformation was also used to reduce the total ground-state energy.⁷¹ In this study, atomic structures of the Au(111) surface were taken from previously resolved global minimum structures on the basis of combined photoelectron spectroscopy measurements.⁷² The slab consisted of three layers (each has 48 Au atoms). We fixed only the bottom layer, and the upper two layers were optimized freely throughout the study. Afterward, we optimized the structure of the IL@Au(111) composite material. The adsorption energies (E_{ads}) of ILs on the Au surface ($E_{\text{ads}}(\text{IL@Au}(111))$) were evaluated using the following equation

Table 4. Calculated Partial Charges (in au) of ([BMIm]⁺[X]⁻) ILs in Gas Phase and for the ([BMIm]⁺[X]⁻)@Au(111) Surface

[BMIm] ⁺ [X] ⁻ where X=		ILs (in gas phase)			ILs@Au(111) surface				
		[BMIm] ⁺	[X] ⁻	total charge of IL	[BMIm] ⁺	[X] ⁻	total charge of IL	total charge of the Au(111) surface	
Cl	Mulliken	0.76	-0.76	0	0.94	-0.32	0.62	-0.62	
	Hirshfeld	0.53	-0.53	0	0.86	0.17	1.02	-1.02	
	Löwdin	0.49	-0.49	0	1.38	0.73	2.11	-2.11	
	Mulliken	0.88	-0.88	0	0.96	-0.49	0.46	-0.46	
DCA	Hirshfeld	0.69	-0.69	0	0.87	-0.27	0.62	-0.62	
	Löwdin	0.67	-0.67	0	1.47	0.35	1.82	-1.82	
	Mulliken	0.73	-0.73	0	0.87	-0.68	0.19	-0.19	
	Hirshfeld	0.72	-0.72	0	0.83	-0.64	0.19	-0.19	
HCOO	Löwdin	0.42	-0.42	0	0.57	-0.41	0.16	-0.16	
	Mulliken	0.88	-0.88	0	0.99	-0.90	0.09	-0.09	
	BF ₄	Hirshfeld	0.97	-0.97	0	1.01	-0.95	0.06	-0.06
	Löwdin	0.56	-0.56	0	1.23	-0.67	0.56	-0.56	
PF ₆	Mulliken	0.90	-0.90	0	0.96	-0.96	0.06	-0.06	
	Hirshfeld	0.98	-0.98	0	0.90	-0.67	0.23	-0.23	
	Löwdin	0.56	-0.56	0	1.09	-0.57	0.52	-0.52	
	Mulliken	0.82	-0.82	0	0.93	-0.70	0.23	-0.23	
CH ₃ SO ₃	Hirshfeld	0.82	-0.82	0	0.90	-0.67	0.23	-0.23	
	Löwdin	0.48	-0.48	0	0.92	-0.42	0.50	-0.50	
	Mulliken	0.89	-0.89	0	1.02	-0.85	0.17	-0.17	
	OTF	Hirshfeld	0.87	-0.87	0	0.97	-0.83	0.14	-0.14
TFSA	Löwdin	0.55	-0.55	0	1.22	-0.56	0.66	-0.66	
	Mulliken	0.88	-0.88	0	0.96	-0.92	0.05	-0.05	
	Hirshfeld	0.90	-0.90	0	0.95	-0.90	0.05	-0.05	
	Löwdin	0.42	-0.42	0	0.90	-0.55	-0.34	-0.34	

$$E_{\text{ads}}(\text{IL}@\text{Au}(111)) = E_{\text{IL}@\text{Au}(111)} - (E_{\text{Au}(111)} + E_{\text{IL}}) \quad (3)$$

where $E_{\text{IL}@\text{Au}(111)}$, $E_{\text{Au}(111)}$, and E_{IL} are the total energies of IL@Au(111), Au(111) surface, and IL, respectively. We have also generated a cube density file from the optimized coordinates (at PBE+D3/TZVP) to study the charge distribution on the surface with ILs.

AUTHOR INFORMATION

Corresponding Authors

*E-mail: prakashspm@gmail.com. Phone: +91 2741 7686. Fax: +91 2745 6702 (M.P.).

*E-mail: hochlaf@univ-mlv.fr (M.H.).

ORCID

Muthuramalingam Prakash: [0000-0002-1886-7708](https://orcid.org/0000-0002-1886-7708)

Gilberte Chambaud: [0000-0002-8031-2746](https://orcid.org/0000-0002-8031-2746)

Notes

The authors declare no competing financial interest.

ACKNOWLEDGMENTS

S.K. acknowledges SRM Institute of Science and Technology (SRM-IST) Research Fellowship for his research work. M.P. thanks the Department of Science and Technology-Science and Engineering Research Board (DST-SERB) of India for the financial support (Grant number: ECR/2017/000891). The authors also thank SRM-IST for providing the supercomputing facility and financial support.

REFERENCES

- Zuo, W.; Ruizhi, L.; Cheng, Z.; Yuanyuan, L.; Jianlong, X.; Jinping, L. Battery-Supercapacitor Hybrid Devices: Recent Progress and Future Prospects. *Adv. Sci.* **2017**, *4*, No. 1600539.
- Sievers, C.; Noda, Y.; et al. Phenomena Affecting Catalytic Reactions at Solid-Liquid Interfaces. *ACS Catal.* **2016**, *6*, 8286–8307.
- Liu, W.; Tkatchenko, A.; Scheffler, M. Modeling Adsorption and Reactions of Organic Molecules at Metal Surfaces. *Acc. Chem. Res.* **2014**, *47*, 3369–3377.
- Lalitha, M.; Lakshmi pathi, S. Interface energies of [EMIm]⁺[X]⁻ and [BMIm]⁺[X]⁻ (X = BF₄, Cl, PF₆, TfO, Tf₂N) based on ionic liquids on graphene, defective graphene, and graphyne surfaces. *J. Mol. Liq.* **2017**, *236*, 124–134.
- Nishi, N.; Minami, K.; Motobayashi, K.; Osawa, M.; Sakka, T. Interfacial Structure at the Quaternary Ammonium-Based Ionic Liquids Gold Electrode Interface Probed by Surface-Enhanced Infrared Absorption Spectroscopy: Anion Dependence of the Cationic Behavior. *J. Phys. Chem. C* **2017**, *121*, 1658–1666.
- Jurado, L. A.; Marzal, R. M. E. Insight into the Electrical Double Layer of an Ionic Liquid on Graphene. *Sci. Rep.* **2017**, *7*, No. 4225.
- Senokos, E.; Ou, Y.; Torres, J. J.; Sket, F.; Gonzalez, C.; Marcilla, R.; Vilatela, J. J. Energy storage in structural composites by introducing CNT fiber/polymer electrolyte interleaves. *Sci. Rep.* **2018**, *8*, No. 3407.
- Navarra, M. A.; Manzi, J.; Lombardo, L.; Panero, S.; Scrosati, B. Ionic Liquid-Based Membranes as Electrolytes for Advanced Lithium Polymer Batteries. *Chem. Sus. Chem.* **2011**, *4*, 125–130.
- Romann, T.; Oll, O.; Kirsimeae, P. K.; Lust, E.; Pikma, P. 4–10 V capacitors with graphene-based electrodes and ionic liquid electrolyte. *J. Power Sources* **2015**, *280*, 606–611.
- Khare, V.; Pham, M. Q.; Kumari, N.; Yoon, H. S.; Kim, C. S.; Park, J. I.; Ahn, S. H. Lubricant for Low Friction and Wear. *ACS Appl. Mater. Interfaces* **2013**, *5*, 4063–4075.
- Liu, C.; Qiu, S.; Dua, P.; Zhao, H.; Wang, L. Ionic liquid-graphene oxide hybrid nanomaterial: synthesis and anticorrosive applications. *Nanoscale* **2018**, *10*, 8115–8124.
- Jorn, R.; Kumar, R.; Abraham, D. P.; Voth, G. A. Atomistic Modeling of the Electrode–Electrolyte Interface in Li-ion Energy Storage Systems: Electrolyte Structuring. *J. Phys. Chem. C* **2013**, *117*, 3747–3761.
- Borodin, O.; Ren, X.; Vatamanu, J.; Cresce, A. V. W.; Knap, K.; Xu, K. Modeling Insight into Battery Electrolyte Electrochemical

- Stability and Interfacial Structure. *Acc. Chem. Res.* **2017**, *50*, 2886–2894.
- (14) Salanne, M. Ionic Liquids for Supercapacitor Applications. *Top. Curr. Chem.* **2017**, *375*, 63.
- (15) Etacheri, V.; Marom, R.; Elazari, R.; Salitra, G.; Aurbach, G. Challenges in the development of advanced Li-ion batteries: a review. *Energy Environ. Sci.* **2011**, *4*, 3243–3262.
- (16) Borisenko, N.; Abedin, S. Z. E. I.; Endres, F. In Situ STM Investigation of Gold Reconstruction and of Silicon Electrode deposition on Au(111) in the Room Temperature Ionic Liquid 1-Butyl-1-methylpyrrolidinium Bis(trifluoromethylsulfonyl)imide. *J. Phys. Chem. B* **2006**, *110*, 6250–6256.
- (17) Pensado, A. S.; Padua, A. A. H.; Comunas, M. J. P.; Fernandez, J. Relationship between Viscosity Coefficients and Volumetric Properties Using a Scaling Concept for Molecular and Ionic Liquids. *J. Phys. Chem. B* **2008**, *112*, 5563–5574.
- (18) Wasserscheid, P.; Welton, T. *Ionic Liquids in Synthesis*, 2nd ed.; Wiley-VCH: Weinheim, Germany, 2007.
- (19) Lewandowski, A.; Galinski, M. Practical and theoretical limits for electrochemical double-layer capacitors. *J. Power Sources* **2007**, *173*, 822–828.
- (20) Wei, D.; Ivaska, A. Applications of ionic liquids in electrochemical sensors. *Anal. Chim. Acta* **2008**, *607*, 126–35.
- (21) Hallett, J. P.; Welton, T. Room-Temperature Ionic Liquids: Solvents for Synthesis and Catalysis. *Chem. Rev.* **2011**, *111*, 3508–3576.
- (22) Watanabe, M.; Thomas, L. M.; Zhang, S.; Ueno, K.; Yasuda, T.; Dokko, K. Application of Ionic Liquids to Energy Storage and Conversion Materials and Devices. *Chem. Rev.* **2017**, *117*, 7190–7239.
- (23) Hayes, R.; Borisenko, N.; Tam, M. K.; Howlett, P. C.; Endres, F.; Atkin, R. Double Layer Structure of Ionic Liquids at the Au(111) Electrode Interface: An Atomic Force Microscopy Investigation. *J. Phys. Chem. C* **2011**, *115*, 6855–6863.
- (24) Yue, Z.; Lele, P.; Zhiwei, F.; Chunshuang, Y.; Xiao, Z.; Guihua, Y. Structural Engineering of 2D Nanomaterials for Energy Storage and Catalysis. *Adv. Mater.* **2018**, *30*, No. 1706347.
- (25) Sobota, M.; Nikiforidis, I.; Hieringer, W.; Paape, N.; Happel, M.; Steinruck, H. P.; Gorling, A.; Wasserscheid, P.; Laurin, M.; Libuda, J. Toward Ionic-Liquid-Based Model Catalysis: Growth, Orientation, Conformation, and Interaction Mechanism of the $[\text{Tf}_2\text{N}]^-$ Anion in $[\text{BMIm}][\text{Tf}_2\text{N}]$ Thin Films on a Well-Ordered Alumina Surface. *Langmuir* **2010**, *26*, 7199–7207.
- (26) Klaver, T. P. C.; Luppi, M.; Sluiter, M. H. F.; Kroon, M. C.; Thijssse, B. J. DFT Study of 1,3-Dimethylimidazolium Tetrafluoroborate on Al and Cu(111) Surfaces. *J. Phys. Chem. C* **2011**, *115*, 14718–14730.
- (27) Buchner, F.; Tonigold, K. F.; Uhl, B.; Alwast, D.; Wagner, N.; Farkhondeh, H.; Grob, A.; Behm, R. J. Toward the Microscopic Identification of Anions and Cations at the Ionic Liquid|Ag(111) Interface: A Combined Experimental and Theoretical Investigation. *ACS Nano* **2013**, *7*, 7773–7784.
- (28) Buchner, F.; Tonigold, K. F.; Bozorgchenani, M.; Gross, A.; Behm, R. J. Interaction of a Self-Assembled Ionic Liquid Layer with Graphite (0001): A Combined Experimental and Theoretical Study. *J. Phys. Chem. Lett.* **2016**, *7*, 226–233.
- (29) Yao, L.; Bing, L.; Shasha, Z.; Yuxia, X.; Huaiguo, X.; Huan, P. Syntheses and Energy Storage Applications of M_xSy (M = Cu, Ag, Au) and Their Composites: Rechargeable Batteries and Supercapacitors. *Adv. Funct. Mater.* **2017**, *27*, No. 1703949.
- (30) Biedron, A. B.; Garfunkel, E. L.; Castner, E. W.; Rangan, S. Ionic liquid ultrathin films at the surface of Cu(100) and Au(111). *J. Chem. Phys.* **2017**, *146*, No. 054704.
- (31) Jhuang, J. Y.; Lee, S. H.; Chen, S. W.; Chen, Y. H.; Chen, Y. J.; Lin, J. L.; Yang, Y. W.; Wang, C. H. Adsorption and Reaction Pathways of 1H-Pyrazole on Cu(100) and O/Cu(100). *J. Phys. Chem. C* **2018**, *122*, 17836–17845.
- (32) Sha, M.; Dou, Q.; et al. Molecular Insights into the Electric Double Layers of Ionic Liquids on Au(100) Electrodes. *ACS Appl. Mater. Interfaces* **2014**, *6*, 12556–12565.
- (33) Wang, R.; Bi, S.; Presser, V.; Feng, G. Systematic comparison of force fields for molecular dynamic simulation of Au(111)/Ionic liquid interfaces. *Fluid Phase Equilib.* **2018**, *463*, 106–113.
- (34) O’Grady, G.; Paskaranandavadiel, N.; Angeli, T. R.; Du, P.; Windsor, J. A.; Cheng, L. K.; Pullan, A. J. A comparison of gold versus silver electrode contacts for high-resolution gastric electrical mapping using flexible printed circuit board arrays. *Physiol. Meas.* **2011**, *32*, N13–N22.
- (35) Bauzá, A.; Frontera, A. Regium- π bonds: An unexplored link between noble metal nanoparticles and aromatic surfaces. *Chem. - Eur. J.* **2018**, *24*, 7228–7234.
- (36) Zierkiewicz, W.; Michalczyk, M.; Scheiner, S. Regium Bonds between Mn Clusters (M = Cu, Ag, Au and n = 2–6) and Nucleophiles NH₃ and HCN. *Phys. Chem. Chem. Phys.* **2018**, *20*, 22498–22509.
- (37) Tariq, M.; Serrob, A. P.; Colac, R.; Saramago, B.; Lopes, J. N. C.; Rebelo, L. P. N. Effect of alkyl chain length on the adsorption and frictional behaviour of 1-alkyl-3-methylimidazolium chloride ionic liquid surfactants on gold surfaces. *Colloids Surf., A* **2011**, *377*, 361–366.
- (38) Pan, G. B.; Freyland, W. 2D phase transition of PF₆ adlayers at the electrified ionic liquid/Au(111) interface. *Chem. Phys. Lett.* **2006**, *427*, 96–100.
- (39) Cremer, T.; Stark, M.; Deyko, A.; Steinruck, H. P.; Maier, F. Liquid/Solid Interface of Ultrathin Ionic Liquid Films: $[\text{C}_1\text{C}_1\text{Im}]$ - $[\text{Tf}_2\text{N}]$ and $[\text{C}_8\text{C}_1\text{Im}]$ - $[\text{Tf}_2\text{N}]$ on Au(111). *Langmuir* **2011**, *27*, 3662–3671.
- (40) Wen, R.; Rahn, B.; Magnussen, O. M. In Situ Video-STM Study of Adlayer Structure and Surface Dynamics at the Ionic Liquid/Au(111) Interface. *J. Phys. Chem. C* **2016**, *120*, 15765–15771.
- (41) Su, Y. Z.; Yan, J. W.; Li, M. G.; Xie, Z. X.; Mao, B. W.; Tian, Z. Q. Adsorption of Solvent Cations on Au(111) and Au(100) in Alkylimidazolium-Based Ionic Liquids - Worm-Like versus Micelle-Like Structures. *Z. Phys. Chem.* **2012**, *226*, 979–994.
- (42) Su, Y.; Yan, J.; Li, M.; Zhang, M.; Mao, B. Electric Double Layer of Au(100)/Imidazolium-Based Ionic Liquids Interface: Effect of Cation Size. *J. Phys. Chem. C* **2013**, *117*, 205–212.
- (43) Su, Y. Z.; Fu, Y. C.; Yan, J. W.; Chen, Z. B.; Mao, B. W. Double Layer of Au(100)/Ionic Liquid Interface and Its Stability in Imidazolium-Based Ionic Liquids. *Angew. Chem., Int. Ed.* **2009**, *48*, 5148–5151.
- (44) Uhl, B.; Huang, H.; Alwast, D.; Buchner, F.; Behm, R. J. Interaction of Ionic Liquids with Noble Metal Surfaces: Structure Formation and Stability of $[\text{OMIm}][\text{TFSA}]$ and $[\text{EMIm}][\text{TFSA}]$ on Au(111) and Ag(111). *Phys. Chem. Chem. Phys.* **2015**, *17*, 23816–23832.
- (45) Tamura, K.; Nishihata, Y. Study on the Behavior of Halide Ions on the Au(111) Electrode Surface in Ionic Liquids Using Surface X-ray Scattering. *J. Phys. Chem. C* **2016**, *120*, 15691–15697.
- (46) Magnussen, O. M. Ordered Anion Adlayers on Metal Electrode Surfaces. *Chem. Rev.* **2002**, *102*, 679–725.
- (47) Salanne, M.; Madden, P. A. Polarization Effects in Ionic Solids and Melts. *Mol. Phys.* **2011**, *109*, 2299–2315.
- (48) Mendonça, A. C. F.; Malfreyt, P.; Padua, A. A. H. Interactions and Ordering of Ionic Liquids at a Metal Surface. *J. Chem. Theory Comput.* **2012**, *8*, 3348–3355.
- (49) Jha, K. C.; Liu, H.; Bockstaller, M. R.; Heinz, H. Facet Recognition and Molecular Ordering of Ionic Liquids on Metal Surfaces. *J. Phys. Chem. C* **2013**, *117*, 25969–25981.
- (50) Liu, Y.; Wang, Y.; Li, J. Molecular dynamics study of confined ionic liquids in Au nanopore. *Ionics* **2016**, *22*, 1681.
- (51) Plöger, J.; Mueller, E. J.; Jacob, T.; Anton, J. Theoretical studies on the adsorption of 1-Butyl-3-methyl-imidazolium-hexafluorophosphate (BMI/PF₆) on Au(100) Surfaces. *Top. Catal.* **2016**, *59*, 792–801.
- (52) Beattie, D. A.; Harmer-Bassell, S. L.; Ho, T. T. M.; Krasowska, M.; Ralston, J.; Sellapperumage, P. M. F.; Wasik, P. Spectroscopic

- study of ionic liquid adsorption from solution onto gold. *Phys. Chem. Chem. Phys.* **2015**, *17*, 4199–4209.
- (53) Beattie, D. A.; Arcifa, A.; Delcheva, I.; Cerf, B. L. A.; Williams, S. V. M.; Rossi, R.; Krasowska, M. Adsorption of Ionic Liquids onto Silver Studied by XPS. *Colloids Surf., A* **2018**, *544*, 78–85.
- (54) Prakash, M.; Chambaud, G.; Al-Mogren, M. M.; Hochlaf, M. Role of size and shape selectivity in interaction between gold nanoclusters and imidazole: a theoretical study. *J. Mol. Model.* **2014**, *20*, 253.
- (55) Prakash, M.; Mathivon, K.; Benoit, D. M.; Chambaud, G.; Hochlaf, M. Carbon dioxide interaction with isolated imidazole or attached on gold clusters and surface: competition between σ H-bond and π stacking interaction. *Phys. Chem. Chem. Phys.* **2014**, *16*, 12503–12509.
- (56) Hu, Z.; Vatamanu, J.; Borodin, O.; Bedrov, D. A comparative study of alkyl imidazolium room temperature ionic liquids with FSI and TFSI anions near charged electrode. *Electrochim. Acta* **2014**, *145*, 40–52.
- (57) Corso, B. L.; Perez, I.; Sheps, T.; Patrick, C. S. O.; Gul, T.; Collins, P. G. Electrochemical Charge-Transfer Resistance in Carbon Nanotube Composites. *Nano Lett.* **2014**, *14*, 1329–1336.
- (58) Atkin, R.; Abedin, S. Z. E.; Hayes, R.; Gasparotto, S.; Borisenco, N.; Endres, F. AFM and STM Studies on the Surface Interaction of [BMP]TFSI and [EMIm]TFSI Ionic Liquids with Au(111). *J. Phys. Chem. C* **2009**, *113*, 13266–13272.
- (59) Lin, L. G.; Wang, Y.; Yan, J. W.; Yuan, Y. Z.; Xiang, J.; Mao, B. W. An in situ STM study on the long-range surface restructuring of Au(111) in a non-chloroaluminated ionic liquid. *Electrochim. Commun.* **2003**, *5*, 995–999.
- (60) Perdew, J. P.; Burke, K.; Ernzerhof, M. Generalized Gradient Approximation Made Simple. *Phys. Rev. Lett.* **1996**, *77*, 3865–3868.
- (61) Grimme, S. Semi empirical GGA-type density functional constructed with a long-range dispersion correction. *J. Comput. Chem.* **2006**, *27*, 1787–1799.
- (62) Grimme, S. Semiempirical hybrid density functional with perturbative second-order correlation. *J. Chem. Phys.* **2006**, *124*, No. 034108.
- (63) Grimme, S.; Antony, V.; Ehrlich, S.; Krieg, H. A consistent and accurate ab initio parametrization of density functional dispersion correction (DFT-D) for the 94 elements H-Pu. *J. Chem. Phys.* **2010**, *132*, No. 154104.
- (64) Frisch, M. J.; Trucks, G. W.; Schlegel, H. B.; Scuseria, G. E.; Robb, M. A.; Cheeseman, J. R.; Scalmani, G.; Barone, V.; Petersson, G. A.; Nakatsuji, H.; Li, X.; Caricato, M.; Marenich, A. V.; Bloino, J. B.; Janesko, G.; Gomperts, R.; Mennucci, B.; Hratchian, H. P.; Ortiz, J. V.; Izmaylov, A. F.; Sonnenberg, J.; Young, L. D. W.; Ding, F.; Lipparini, F.; Egidi, F.; Goings, J.; Peng, B.; Petrone, A.; Henderson, T.; Ranasinghe, D.; Zakrzewski, V. G.; Gao, J.; Rega, N.; Zheng, G.; Liang, W.; Hada, M.; Ehara, M.; Toyota, K.; Fukuda, R.; Hasegawa, J.; Ishida, M.; Nakajima, T.; Honda, Y.; Kitao, O.; Nakai, H.; Vreven, T.; Throssell, K.; Montgomery, J. A.; Peralta, J. E.; Ogliaro, F.; Bearpark, M. J.; Heyd, J. J.; Brothers, E. N.; Kudin, K. N.; Staroverov, V. N.; Keith, T. A.; Kobayashi, R.; Normand, J.; Raghavachari, K.; Rendell, A. P.; Burant, S.; Iyengar, S.; Tomasi, J.; Cossi, M.; Millam, J. M.; Klene, M.; Adamo, C.; Cammi, R.; Ochterski, J. W.; Martin, R. L.; Morokuma, K.; Farkas, O.; Foresman, J. B.; Fox, D. J. *G16 RevA.03*; Gaussian, Inc.: Wallingford CT, 2016.
- (65) Hay, P. J.; Wadt, W. R. Ab initio effective core potentials for molecular calculations Potentials for K to Au including the outermost core orbitals. *J. Chem. Phys.* **1985**, *82*, 299.
- (66) Boys, S. F.; Bernardi, F. The calculation of small molecular interactions by the differences of separate total energies. Some procedures with reduced errors. *Mol. Phys.* **1970**, *19*, 553–566.
- (67) VandeVondele, J.; Krack, M.; Mohamed, F.; Parrinello, M.; Chassaing, T.; Hutter, J. QUICKSTEP: Fast and accurate density functional calculations using a mixed Gaussian and plane waves approach. *Comput. Phys. Commun.* **2005**, *77*, 103–128.
- (68) Lippert, G.; Hutter, J.; Parrinello, M. The Gaussian and augmented-plane-wave density functional method for ab initio molecular dynamics simulations. *Theor. Chem. Acc.* **1999**, *103*, 124–140.
- (69) Lippert, B. G.; Hutter, J.; Parrinello, M. A hybrid Gaussian and plane wave density functional scheme. *Mol. Phys.* **1997**, *92*, 477–487.
- (70) VandeVondele, J.; Hutter, J. Gaussian basis sets for accurate calculations on molecular systems in gas and condensed phases. *J. Chem. Phys.* **2007**, *127*, No. 114105.
- (71) VandeVondele, J.; Hutter, J. An efficient orbital transformation method for electronic structure calculations. *J. Chem. Phys.* **2003**, *118*, 4365–4369.
- (72) Nguyen, M. T.; Pignedoli, C. A.; Treier, M. R.; Fasel, R.; Passerone, D. The role of van der Waals interactions in surface-supported supramolecular networks. *Phys. Chem. Chem. Phys.* **2010**, *12*, 992–999.